UV Resonance Raman Examination of the Azurin Tryptophan Environment and Energy Relaxation Pathways

Joyce A. Sweeney,[†] Paul A. Harmon,[†,‡] Sanford A. Asher,*[,†] Cindy M. Hutnik,[§] and Arthur G. Szabo[§]

Contribution from the Department of Chemistry, University of Pittsburgh, Pittsburgh, Pennsylvania 15260, and the Division of Biological Sciences, National Research Council of Canada, Ottawa, Canada K1A 0R6. *Received October 12, 1990*

Abstract: We utilize the new technique of resonance Raman saturation spectroscopy to investigate the role of tryptophan-48 (Trp) in the electron-transfer processes in azurin from *Pseudomonas aeruginosa* (*Pae*). Ultraviolet resonance Raman saturation (UVRR) studies probe ground electronic state recovery rates via the nonlinear dependence of ground-state resonance Raman (RR) intensities on the laser excitation energy flux. These studies allow us to extract the Trp T_1 relaxation rates. Our RR saturation studies of azurin indicate that the Trp-48 fluorescing excited states relax in less than 200 ps back to the ground state. Further, the ground-state recovery rates we measure are identical, within experimental error, to the fluorescing excited-state decay rates as measured by time resolved fluorescence techniques. These results argue strongly against the recently proposed mechanism for the Trp fluorescence quenching in azurin, which involves formation of a Trp radical cation intermediate. Our Trp ground-state recovery data are consistent with a simple energy transfer fluorescence quenching mechanism.

Introduction

The blue-copper protein azurin represents an essential component of certain bacterial electron-transport chains. Azurin from *Pseudomonas aeruginosa* (*Pae*) is a 14000-dalton protein containing 128 amino acids.[1] The redox active site of native *Pae* azurin contains a single oxidized copper ion bound in a distorted tetrahedral fashion to four amino acid residues, His-46, His-117, Cys-112, and Met-121. A single Trp residue at position 48 is located inside an extremely hydrophobic barrel region formed by eight β-strands. This Trp residue is ca. 9 Å away from the copper redox site[2] and may play a role in electron-transfer processes.[3-7]

Physiologically, azurin functions as an electron carrier in a bacterial respiratory chain with cytochrome c_{551} as the most probable redox partner.[8] The molecular details of the electron-transfer mechanism for azurin have not been fully elucidated. However, the X-ray crystallographic structures for *Pae* azurin[9] and *Alcaligenes*[10] *denitrificans* suggest the locations of probable-electron-transfer conduits (e.g. metal redox sites and disulfide bridges in relation to the π systems of aromatic amino acids). The presence of aromatic amino acids in electron-transfer pathways are thought to increase electron-transfer rates by enhancing electronic couplings between donor and acceptor species.[3-5,7]

Studies of the electron-transfer conduits are important to develop a detailed understanding of electron-transfer mechanisms in proteins. Experimentally, electron-transfer processes can be examined by adding exogenous oxidants and reductants or by using photons to try to induce electron transfer.[4,11] For azurin numerous studies have concentrated on Trp-48 because it may be involved in electron trnasfer to the Cu site.[3,5,7] Many of the unique absorption and fluorescence spectral features of *Pae* azurin (as well as *Pseudomonas fluorescens* ATCC-13525-2 (*Pfl*) azurin[5,7]) can be attributed to this single Trp residue.[3,5,12-15]

Several groups have investigated the Trp fluorescence behavior in azurins from different bacterial strains with the expectation of characterizing the Trp environment and interactions between the Trp and potential redox partners involved in the electron-transfer conduit.[3,5,7,12,13] They find at least double exponential decay kinetics for the Trp of *Pae* and *Pfl* holoazurins. More recently, Hutnik and Szabo report multiexponential decay kinetics which are indicative of three distinct lifetime components in the *Pae* and *Pfl* holo and Cu(II)- or Cu(I)-reconstituted azurins.[3] These different decay components could be due to different Trp environments. However, Petrich et al. question the physiological relevance of the multiexponential decay because they attribute the long lifetime component of their observed double exponential decay for *Pae* azurin to an "apo-like" contaminant.[5] All groups except Munro et al.[13] report a single exponential decay for apoazurins from these strains.

The Trp fluorescence quantum yield dramatically increases in apoazurin compared to holoazurin.[3,5,7,12,13] The origin of the holoazurin quenching may indicate particular Trp–protein residue interactions. Szabo et al. propose the existence of holoazurin conformers in which the distance between the Trp residue and the putative quencher, the copper–ligand complex, varies, resulting in three distinct fluorescence decay time components.[7] A likely fluorescence quenching mechanism which relies on distance as well as orientation of the chromophores is Förster energy transfer. Fleming and co-workers also investigated this quenching; in view of their fluorescence studies and their calculations of likely electron-transfer rates in azurin from the first excited singlet state of Trp to Cu(II), they concluded that the quenching derives from electron transfer and the formation of an excited-state Trp radical cation product.[5] More recently, the Fleming group[6] investigated the possibility of a Förster energy-transfer quenching mechanism for Trp in *Pae* and *Afe* (*Alcaligenes faecalis*) azurins, as well as in various metal derivatives. Although they found acceptable

* Author to whom correspondence should be addressed.
† University of Pittsburgh.
‡ Present address: National Institutes of Health, Bethesda, MD 20892.
§ National Research Council of Canada.

(1) Ambler, R. P. In *Recent Developments in the Chemical Studies of Protein Structures*; Previero, A., Perchere, J. F., Coletti-Previero, M. A., Eds.; INSERM Press: Paris, 1973; pp 289-305.
(2) Ugurbil, K.; Norton, R. S.; Allerhand, A.; Bersohn, R. *Biochemistry* **1977**, *16*, 886-894.
(3) Hutnik, C. M.; Szabo, A. G. *Biochemistry* **1989**, *28*, 3923-3934.
(4) Farver, O.; Pecht, I. *Proc. Natl. Acad. Sci. U.S.A.* **1989**, *86*, 6968-6972.
(5) Petrich, J. W.; Longworth, J. W.; Fleming, G. R. *Biochemistry* **1987**, *26*, 2711-2722.
(6) Hansen, J. E.; Longworth, J. W.; Fleming, G. R. *Biochemistry* **1990**, *29*, 7329-7338.
(7) Szabo, A. G.; Stepanik, T. M.; Wayner, D. M.; Young, N. M. *Biophys. J.* **1983**, *41*, 233-244.
(8) Rosen, P.; Pecht, I. *Biochemistry* **1976**, *15*, 775.
(9) Adman, E. T.; Stenkamp, R. E.; Sieker, L. C.; Jensen, L. H. *J. Mol. Biol.* **1978**, *123*, 35-47.
(10) Norris, G. E.; Anderson, B. F.; Baker, E. N. *J. Mol. Biol.* **1983**, *165*, 501-521.
(11) Corin, A. F.; Gould, I. R. *Photochem. Photobiol.* **1989**, *50*, 413-418.
(12) Grinvald, A.; Schlessinger, J.; Pecht, I.; Steinberg, I. Z. *Biochemistry* **1975**, *14*, 1921.
(13) Munro, I.; Pecht, I.; Stryer, L. *Proc. Natl. Acad. Sci.* **1979**, *76*, 56.
(14) Burnstein, E. A.; Permyakov, E. A.; Yashin, V. A.; Burkhanov, S. A.; Finazzi-Agro, A. *Biochim. Biophys. Acta* **1977**, *491*, 155.
(15) Finazzi-Agro, A.; Giovagnoli, C.; Avigliano, L.; Rotilio, G.; Mondovi, B. *Eur. J. Biochem.* **1973**, *34*, 20.

0002-7863/91/1513-7531$02.50/0

agreement for Cu(II) *Afe* azurin and for three metal derivatives [Ni(II), Co(II), and Hg(II)] of *Pae* azurin, the calculated rate constants were not suggestive of Förster energy transfer for Cu(II) and Cu(I) *Pae*, Ag(I) *Pae*, and Cu(I) *Afe* azurins. Hansen et al.[6] were unable to reach a firm conclusion for the mechanism of fluorescence quenching in these species and concluded that electron transfer may play a major role in the Trp fluorescence quenching.[6]

In the work here we use the technique of resonance Raman saturation spectroscopy (RSS), recently developed in our laboratory,[16,17] to investigate the excited-state Trp relaxation rates in holoazurin as well as the apo and denatured proteins. This Raman technique examines excited-state relaxation processes of specific amino acids by using the intensity of the ground-state Raman bands to monitor the population of the ground-state species during the incident laser pulse. This incident excitation pulse transfers some of the ground-state population into electronic excited states. In contrast to fluorescence measurements which only monitor the relaxation from the lowest singlet state, RRSS monitors evolution directly from *all* intermediate states back to the ground state. Thus, it can monitor other channels such as those caused by photoionization and radical cation formation. In addition, RRSS can monitor relaxation processes in tyrosine (Tyr) and phenylalanine (Phe) due to the vibrational resolution inherent in Raman spectroscopy. The broad fluorescence bands and the overlap with Trp emission make it impossible to study these residues with time-resolved fluorescence spectroscopic techniques.

The present study focuses on the excited-state relaxation pathways of Trp-48 in *Pae* azurin. Our results rule out the formation of Trp radical cation. Instead, we observe Trp ground-state recovery rates for holoazurin which agree with excited-state relaxation rates determined by fluorescence studies. This indicates that the fluorescence quenching derives directly from energy transfer from Trp to the Cu–ligand complex.

Experimental Section

Materials. Holoazurin from *Pseudomonas aeruginosa* (*Pae*) was purified by modifications[3,7] of the procedure of Ambler and Wynn.[18] *N*-Acetyltryptophanamide (NATA), *N*-acetyltyrosinamide (NATyrAm) (Sigma Chemical Co.), cacodylic acid (Aldrich Chemical Co.), cupric chloride dihydrate (EM Science), and potassium cyanide (Fisher Scientific) were used without further purification. Imidazole (Aldrich) was sublimed before use. Spectrapor dialysis tubing (MWCO 3500, Fisher Scientific) was presoaked in 100 mM cacodylic acid buffer, pH 6, containing 6 M guanidine hydrochloride (Aldrich Chemical Co.) for use in the denaturation procedure.

Methods. The *Pae* holoazurin showed an absorption spectral ratio (A_{620}/A_{280}) of 0.54 confirming sample homogeneity.[3] The purified azurin sample was concentrated with use of an Amicon concentrator, Model 8050, with a diaflow ultrafilter YM2 (MWCO 1000). Resuspension of the holoazurin in a cacodylic acid buffer at pH 6 gave a final azurin concentration of 75 μM and a cacodylic acid concentration of 100 mM. Cacodylic acid was used as the Raman internal intensity standard.

Apoazurin was prepared from holoazurin with use of the KCN dialysis procedure of Yamanaka et al.,[19] but as modified by Hutnik and Szabo.[3] At room temperature, 19.0 mL of holoazurin was dialyzed against 2.7 L of 100 mM phosphate buffer, pH 7.3, for 2 h. The sample was further dialyzed against 1.0 L of 100 mM phosphate buffer containing 0.5 M KCN, pH 8.5, at room temperature. This dialysis was terminated after ca. 30 min when the solution inside the dialysis tubing was clear (i.e. no blue color). Dialysis at 4 °C against 100 mM cacodylic acid buffer, pH 6, with two buffer changes occurred over a 25-h period.

Cu(II)-reconstituted azurin was prepared[3] by dialyzing apoazurin at 4 °C against 100 mM cacodylic acid buffer, pH 6, containing a 10-fold molar excess of cupric chloride. The sample-to-dialysis buffer volume ratio was 1:129. The contents of the dialysis bag turned blue after 30 min, but dialysis was continued for an additional 30 min to ensure complete uptake of the cupric ion. The sample was subsequently dialyzed against 2.0 L of 100 mM cacodylic acid buffer, pH 6, for ca. 18 h at 4 °C to remove the excess cupric ion.

Cu(II)-reconstituted azurin was reduced to Cu(I) azurin by the addition of a small excess of 0.4 M sodium dithionite to a 2.56×10^{-4} M solution of Cu(II) azurin. A total loss of blue color occurred in less than 1 min. The sodium dithionite was removed by further dialysis. The absorption at 625 nm decreased by 82%.

Cu(II)-reconstituted azurin was denatured by dialysis against 6 M Gd-HCl in 100 mM cacodylic acid buffer, pH 6. The Gd-HCl was removed by extensive dialysis against cacodylic acid buffer prior to the absorption and Raman measurements. The loss of the sharp Trp vibronic feature at ca. 291 nm in the absorption spectrum of the denatured azurin after the removal of Gd-HCl indicates that the single Trp at position 48 becomes at least partially exposed to aqueous solvent.[7,12]

The Cu(II)–(imidazole)$_4$ complex was prepared by mixing the aqueous imidazole and Cu(II) solutions. The ligand dissociation of the complex should be less than 10%.[20]

The holoazurin, apoazurin, and denatured azurin concentrations used for the Raman experiments were 75.0, 62.5, and 59.3 μM, respectively. The Raman saturation study used the saturation behavior of NATA to calibrate the incident laser energy flux.[16] NATA concentrations were adjusted to obtain an absorbance at the laser line identical with that of the azurin excited in the Raman experiment. This ensures the same laser beam penetration depth (i.e. identical illuminated sample volumes) for both NATA and azurin during the Raman measurement. The 605-cm^{-1} band of cacodylic acid was used as the internal intensity standard; Song and Asher[21] recently demonstrated that cacodylic acid Raman bands do not show photochemistry or saturation with 225-nm excitation for incident flux energies below 1000 mJ/cm^2.

Instrumentation. The incident laser excitation was generated by doubling the 1.06-μm fundamental of a Quanta-Ray DCR-2A Nd:YAG laser to pump fluorescein 548 in a Quanta Ray PDL dye laser. The laser pulse width is ca. 4–6 ns emitting at a 20-Hz-repetition rate. The output of the dye laser is frequency-doubled and mixed by using a Quanta Ray WEX unit. The wavelength for Raman excitation in this study is 225 nm. The continuous flow sampling system used a Buchler Multistaltic pump which recirculates the 2.0-mL-sample volume through a Suprasil quartz capillary tube (1.0-mm i.d.). The sample volume is replenished between laser pulses. The incident laser beam spot size at the sample is ca. 1 mm^2. The energy flux (±15%) at the sample is determined by using a NATA calibration standard as described elsewhere.[16]

The Raman scattered light is collected in a back-scattering geometry by an ellipsoidal mirror and imaged onto the entrance slit of a Spex Triplemate monochromator. A 1200-groove/mm UV grating in the spectograph stage of the monochromator gave a spectral resolution of ca. 29 cm^{-1}. An EG&G PAR 1420 blue-intensified Reticon diode array interfaced to a PAR Model 1215 OMA II or Model 1460 OMA III data station detects the dispersed light. The throughput efficiencies of the monochromator and detector in the UV wavelength region were determined by using a standard intensity deuterium lamp scattered from a Lambert surface prepared from Kodak White Reflectance Standard. The intensified Reticon detector pixel sensitivity was determined by translating a narrow wavelength band (<1 nm) across the pixel array. All of the cross sections were corrected for the variation in pixel sensitivity.

The relative intensities of the Trp bands to the cacodylic acid internal intensity standard Raman bands were obtained by measuring the relative peak heights. Raman cross sections were determined from relative intensity ratios extrapolated to zero flux on Raman saturation plots (relative intensity versus incident energy flux) according to the method of Johnson et al.[22] Quantitative Raman cross sections for Trp and cacodylic acid vibrational bands are derived from the absolute Raman cross sections of perchlorate previously determined by Dudik et al.[23] Corrections for monochromator and detector wavelength efficiency biases and pixel sensitivity across the diode array are incorporated into the cross section calculations. Intensity contributions of tyrosine, phenylalanine, and/or cacodylate were deconvoluted from the Trp bands. Total corrections were less than ca. 10%.

The absorption spectra were measured by using a Perkin-Elmer Lambda 9 UV–vis–near-IR spectrophotometer.

Results

UV Resonance Raman Saturation. We determined Trp excited-state lifetimes in azurin using the new technique of Raman

(16) Teraoka, J.; Harmon, P. A.; Asher, S. A. *J. Am. Chem. Soc.* **1990**, *112*, 2892–2900.
(17) Harmon, P. A.; Teraoka, J.; Asher, S. A. *J. Am. Chem. Soc.* **1990**, *112*, 8789–8799.
(18) Ambler, R. P.; Wynn, M. *Biochem. J.* **1973**, *131*, 485.
(19) Yamanaka, T.; Kijimoto, S.; Okunuki, K. *J. Biochem.* **1963**, *53*, 256.
(20) Caswell, D. S.; Spiro, T. G. *J. Am. Chem. Soc.* **1986**, *108*, 6470–6477.
(21) Song, S.; Asher, S. A. *Biochemistry* **1991**, *30*, 1199–1205.
(22) Johnson, C. R.; Ludwig, M.; Asher, S. A. *J. Am. Chem. Soc.* **1986**, *108*, 905.
(23) Dudik, J. M.; Johnson, C. R.; Asher, S. A. *J. Chem. Phys.* **1985**, *82*, 1732–1740.

Table I. Azurin Trp Raman Cross Sections and the Excited-State Lifetimes Obtained from Ground-State Repopulation Rates and Fluorescence Studies of Trp in *Pae* Azurin

	fluorescence[a]							Raman saturation spectroscopy		
sample	τ_1, ns	τ_2, ns	τ_3, ns	τ,[g] ns	α_1	α_2	α_3	ν_{obs}, cm^{-1}	τ,[f] ns	σ,[d] b/mole·sr
holoazurin	4.89	0.36	0.10	0.21	0.02	0.05	0.93	755	<0.2 ± 0.1	1.1
								1007	<0.2 ± 0.1	1.2
apoazurin	5.08				100			755	4.0 ± 2.0	1.8
								1007	4.9 ± 2.4	1.6
denatured azurin (*Pae*)	N.A.				N.A.			755	3.0 ± 1.5	1.4
								1007	1.8 ± 0.9	1.2
NATA								760	2.9 ± 0.5[e]	2.1
								1009		
Trp								760	2.4 ± 0.3[e]	2.5
								1009		2.0
denatured azurin[b] (*Pfl*)	2.99	0.76		1.65	0.40	0.60				
denatured azurin[c] (*Pfl*)	3.4	1.2		2.04	0.38	0.62				

[a] Reference 3. [b] Reference 7. [c] Reference 12. [d] 225-nm excitation. [e] Reference 16. [f] Excited state lifetimes obtained from ground-state repopulation rates. [g] Weighted average of the fluorescence lifetimes for all components.

saturation spectroscopy (RSS).[16,17] This technique monitors the ground-state depletion of Trp residues through the intensities of the Trp Raman bands. Depletion of the Trp ground-state population can be described by the following rate equation[16,22]

$$-(dP/dt) = \sigma_A I(t)P - KP^* \quad (1)$$

where P is the ground-state population, P^* is the population of the thermalized fluorescing levels, σ_A is the absorption cross section of the ground-state molecules, and $I(t)$ is the laser pulse flux density which includes the integrated energy flux per pulse times the temporal pulse shape function (assumed to be rectangular).[16]

The dependence of the Raman intensity ratio of the Trp band relative to that of a non-absorbing internal standard is given by eq 8 of Teraoka et al.[16] for relaxation through a single channel.

$$\frac{I_{RR}}{I_s} = \frac{\sigma_R P_0}{\sigma_S C_0(\sigma_A I_0 + Kt_0)^2}\{(Kt_0)^2 + \sigma_A I_0(1 + Kt_0 - \exp[-(\sigma_A I_0 + Kt_0)])\} \quad (2)$$

A more complex expression would occur (eq 11 from ref 16) if an additional channel existed such as a photoionization process.[16] The relative Raman intensity of a Trp Raman band (I_{RR}) relative to that of an internal standard (I_s) depends upon known quantities such as the concentrations of Trp (P_0) and internal standard (C_0), the Raman cross sections of Trp (σ_R) and the internal standard (σ_S), and the Trp absorption cross section (σ_A). I_0 is the integrated pulse energy flux and t_0 is the temporal pulse length. We determine the Trp ground-state repopulation rate (K) (which for *Pae* azurin appears identical with the reciprocal Trp excited-state lifetime) by fitting eq 2 above to the Raman saturation data.

The measurement is conducted in an extremely low energy flux regime to avoid excited-state absorption and/or photon-driven relaxations. When this condition is achieved, the rate constant K determines the T_1 repopulation rate of the ground state and thus the Raman intensity. The reciprocal of K is identical with the S_1 excited-state lifetime when all relaxation occurs through the S_1 state. The lifetime resolution of RRSS is limited by the signal-to-noise ratio of the Raman spectra which must be obtained in a low incident energy flux regime.

The excited-state lifetimes of Trp in *Pae* azurin and its modified forms as determined by this technique are listed in Table I, which also lists the corresponding fluorescence lifetime values. A rough statistical analysis shows an error of ca. 50% for the Trp azurin excited state lifetime values. Our present signal-to-noise ratios for the Raman Saturation spectroscopy do not allow us to distinguish similar multiple lifetime components in a sample. We detect the weighted average lifetime of these components. If one component dominates, the excited-state lifetime obtained will essentially be that of this component.

Figure 1 shows the 225 nm excited Raman spectra of holoazurins, apoazurins, and denatured *Pae* azurins. The Raman saturation plots in Figure 2 for the Trp 755 and 1007-cm^{-1} bands derive from 225-nm Raman spectra obtained with incident energy

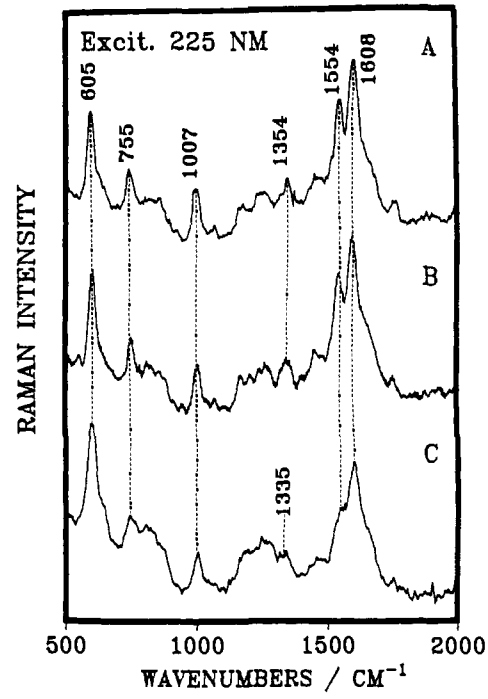

Figure 1. 225-nm excited UV-resonance Raman spectra of (A) holoazurin (7.5 × 10^5 M, 26.6 mJ/(pulse·cm^2)), (B) apoazurin (6.25 × 10^{-5} M, 15.4 mJ/(pulse cm^2)), and (C) denatured azurin (5.93 × 10^{-5} M, 14.9 mJ/(pulse·cm^2)). The holoazurin spectrum shows negligible Raman saturation, while the displayed apo and denatured azurins show significant saturation. The Raman cross sections were determined from the intercept of the Raman saturation plots of Figure 2.

flux densities ranging from 1 to 26 mJ/cm^2. The relative ratio of the Trp Raman intensity to the 605-cm^{-1}-band internal standard cacodylate intensity is plotted versus incident pulse energy flux. The solid lines are nonlinear least-squares fits of the data to the saturation expression[16] which allows us to calculate the T_1 relaxation rates. Qualitatively, the steepness of the curve reflects the ground-state repopulation rate and thus the reciprocal of the excited-state lifetime. Holoazurin has the flattest curve, indicating the fastest ground-state recovery; negligible Trp saturation is observed at even the highest energy flux values. The excited-state lifetime for Trp in holoazurin is determined to be less than 200 ps, and this value is close to the measured Trp fluorescence lifetime (ca. 100 ps) of the dominating shortest lived component of holoazurin which accounts for 93% of the Trp fluorescence.[3]

The agreement between the fluorescence lifetime and the reciprocal ground-state recovery rate (T_1) eliminates the possibility of formation of a long-lived Trp radical cation as a result of electron transfer. This conflicts with Fleming and co-workers' earlier proposal that the Trp fluorescence quenching in azurin

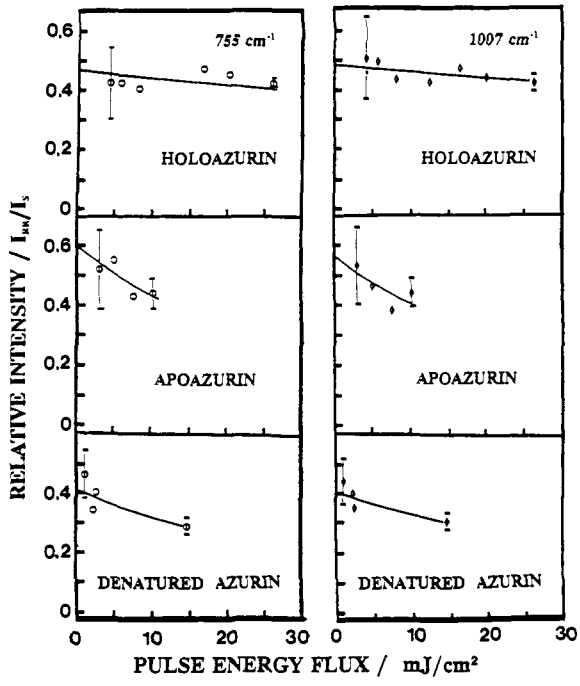

Figure 2. Raman saturation plots of the 755- and 1007-cm^{-1} Trp intensities relative to the 605-cm^{-1} cacodylate internal standard intensity versus incident pulse energy flux. The solid curves show the nonlinear least-squares fits to the data. Representative error bars are shown for the best and worst S/N data point.

derived from formation of the Trp radical cation and the reduction of Cu(II).[5] Although their recent calculations suggest that Förster energy transfer could dominate the quenching for numerous azurin derivatives, their calculations for Cu(II) and Cu(I) *Pae* azurin are not indicative of Förster transfer. They are unable to reach a definitive conclusion regarding the *Pae* quenching mechanism.

The apoazurin shows the steepest saturation curve (Figure 2), reflecting the slowest ground-state recovery of ca. 1/4.5 ns^{-1}. The kinetic fluorescence data for apoazurin shows a single exponential fluorescence decay curve, with a lifetime of 5 ns. The agreement between fluorescence lifetime data and the reciprocal ground-state recovery rate is excellent.

The denatured azurin shows an intermediate slope which reflects a weighted average liftime of 2.4 ns for the different conformational components as indicated by its multiexponential fluorescence decay kinetics. We see only a weighted average because no particular component dominates the composition.

We were careful to minimize the UV illumination of the azurin samples and to use spectra from samples which did not show extensive photochemical alterations. These precautions ensured that our excited-state lifetimes derived from first-order excited-state relaxation processes. However, absorption spectra of holoazurin samples obtained after extensive laser excitation with energy flux values greater than 15 mJ/(pulse·cm^2) show laser-induced reduction of the azurin, probably resulting from photoionization of the S_3 singlet. This observation is reminiscent of the absorption spectral changes observed when holoazurin is chemically reduced. We see a decrease in the absorbance of the 625-nm $\sigma_{S(cys)} \rightarrow$ Cu(II) $d_{x^2-y^2}$ charge-transfer band[24] and an approximately 45% increase in the absorbance of the broad near-UV band (250–300 nm). However, this photochemical reduction does not result in the characteristic red-shift for the sharp Trp vibrational feature at ca. 291 nm seen upon chemical reduction. Under aerobic conditions the protein reoxidizes to its original form.

Absorbance. Figure 3 shows the near-UV absorption spectra of oxidized and reduced azurin as well as the difference spectrum.

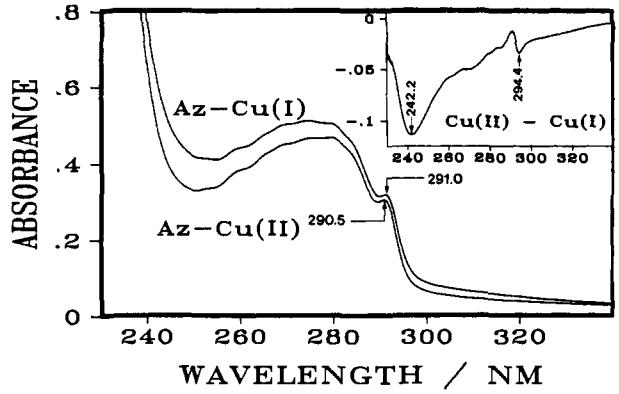

Figure 3. Absorption spectra of oxidized and reduced *Pae* azurin (2.56 × 10^{-4} M). The cell path length is 0.2 cm. The inset displays the absorption difference spectrum between oxidized and reduced azurin.

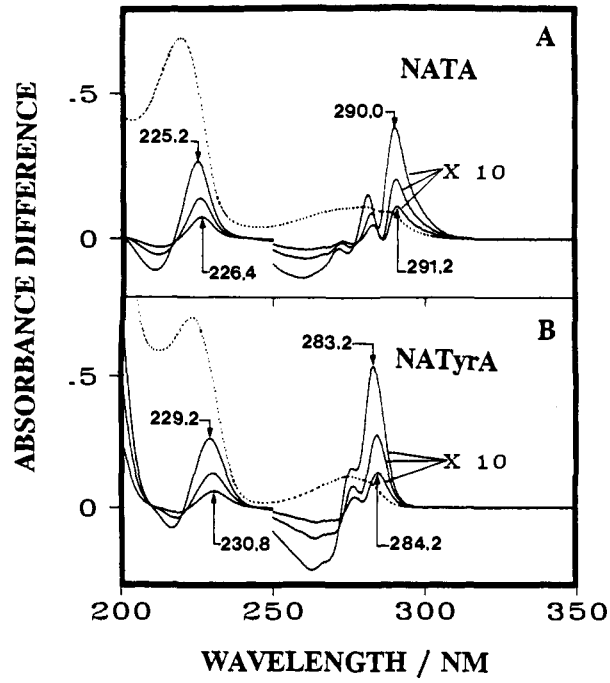

Figure 4. (A) Absorption spectrum of a 1.0 × 10^{-4} M *N*-acetyltryptophanamide (NATA) solution in water for a path length of 0.2 cm (dotted line). Also shown are difference spectra between NATA spectra which have been numerically blue shifted by 1, 2, and 4 nm. (B) Absorption spectrum of a 4.0 × 10^{-4} M *N*-acetyltyrosinamide (NATyrA) solution in water for a path length of 0.2 cm (dotted line). Also shown are difference spectra between NATyrAm spectra which have been blue shifted by 1, 2, and 4 nm.

The difference spectrum resembles that of Hansen et al.[6] and Pecht et al.[25] The sharp band which red shifts from 290.5 to 291.0 nm upon reduction of the copper ion[7,25] derives from the Trp 0–0 ^1L_b transition.[26-29] This narrow feature is absent for azurin from *Pseudomonas fluorescens*, ATCC 13430, which lacks Trp.[30] The absorbance of reduced Cu(I) azurin in the spectral region between 250 and 300 nm is increased compared to that of the Cu(II) oxidized form, and a strong difference spectral feature occurs at 242 nm. We are unsure whether this broad difference spectral feature results from an overall increased molar absorptivity of the aromatic amino acid absorption bands in the reduced protein or whether it derives from an increased absorbance of the Cu(I)–ligand complex compared to that of the Cu(II) complex in this

(24) Solomon, E. I.; Hare, J. W.; Dooley, D. M.; Dawson, J. H.; Stephens, P. J. *J. Am. Chem. Soc.* **1980**, *102* (1), 168.

(25) Pecht, I.; Farver, O.; Goldberg, M. *Adv. Chem. Ser.* **1977**, *162*, 179–206.
(26) Valeur, B.; Weber, G. *Photochem. Photobiol.* **1977**, *25*, 441–444.
(27) Martinaud, M.; Kadiri, A. *Chem. Phys.* **1978**, *28*, 473–485.
(28) Meech, S. R.; Phillips, D.; Lee, A. G. *Chem. Phys.* **1983**, *80*, 317–328.
(29) Strickland. E. H.; Billups, C. *Biopolymers* **1973**, *12*, 1989–1995.
(30) Ugurbil, K.; Bersohn, R. *Biochemistry* **1977**, *16*, 895–901.

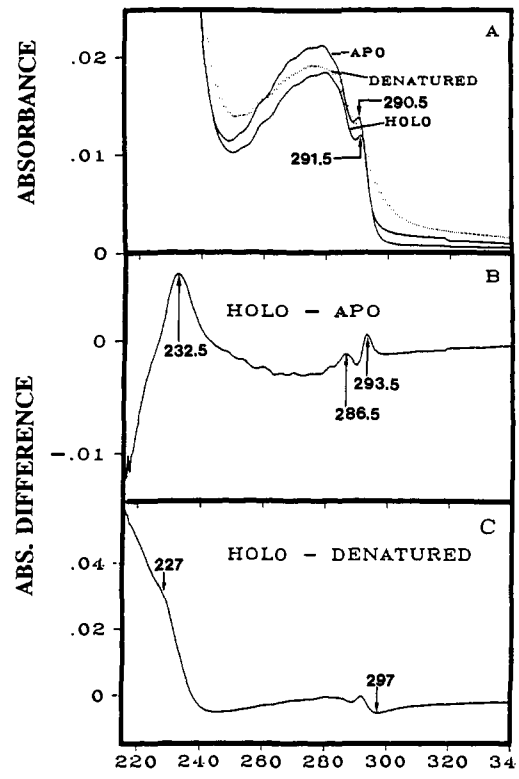

Figure 5. (A) Absorption spectra of *Pae* holoazurin, apoazurin, and Gd-HCl denatured azurin (1.0×10^{-5} M, 0.2 cm path length). Absorption (spectra were normalized for concentration in order to display them on the same ordinate scale. (B) Absorption difference spectra between holoazurin and apoazurin and (C) between holoazurin and denatured azurin.

spectral region. The red shift in the Trp ^1L_b transition upon copper reduction, however, indicates communication of the oxidation change to the Trp. This communication could occur electrostatically, through a local environment change, or through a change in coupling of the Trp electronic transition with transitions of the Cu ligands (vide infra).

Figure 4A shows the absorption spectrum of NATA (dotted line) and difference spectra (solid lines) between the normal NATA absorption spectrum and NATA spectra which have been numerically blue shifted by 1 to 4 nm. The blue shift results in difference spectral features at ca. 291 and 226 nm for the Trp ^1L_b and ^1B_b bands, respectively. This ca. 291-nm difference spectral peak appears as a trough at 294.4 nm in the oxidized minus reduced spectrum of Figure 3, indicating a red shift for the Trp 0–0 ^1L_b upon reduction of holoazurin. There is no feature in the Figure 4A difference spectra that can be related to the 242.2-nm Cu(II)–Cu(I) difference spectral trough in Figure 3 (inset). In addition, Figure 4B shows NATyrAm absorption and difference spectral features. Obviously, Tyr spectral shifts also cannot account for this 242.2-nm azurin band. Thus, we suggest that this spectral feature derives from a change in the absorbance of the Cu–ligand complex (vide infra).

Figure 5A compares the absorption spectra of native holoazurin, apoazurin (Cu removed), and denatured azurin. The broad 250–300-nm band has contributions from the ^1L_b transitions of Tyr and Phe as well as from the ^1L_a and ^1L_b transitions of Trp. The apoazurin spectrum in Figure 5A shows a blue shift of the Trp 0–0 ^1L_b feature from 291.5 nm in holoazurin to 290.5 nm in apoazurin. This Trp vibronic feature is known to be narrow for Trp in hydrophobic environments. For example, Szabo et al.[7] and Meech and Phillips[28] observe this sharp vibronic feature for 3-methylindole in nonpolar solvents and show its disappearance in an aqueous environment (possibly due to a red shift of the solvent-sensitive ^1L_a transition to broaden this band).[28] Since this Trp 0–0 ^1L_b band remains sharp in both oxidized and reduced azurin as well as in apoazurin it appears that the Trp local environment remains hydrophobic in these protein forms.[7] The disappearance of this narrow band in denatured azurin (Figure 5A) suggests that the Trp has become exposed to the aqueous solution.[7] The denatured azurin absorption spectrum was obtained after removal of the guanidine hydrochloride (Gd-HCl) by exhaustive dialysis at 4 °C. Thus, the protein may not be completely unfolded but upon denaturant removal may refold to a non-native form.

The Figure 5B difference spectrum of holoazurin minus apoazurin shows a maximum at 293.5 nm (L_1) which must derive from a ca. 1 nm blue shift for the apoazurin Trp ^1L_b transition. The peak at 286.5 nm (L_2) in the difference spectrum may partially derive from a blue shifted apoazurin Tyr transition (Figure 4B). The difference spectrum between the holoazurin and denatured azurin is much more complex because of the increased width of the denatured protein in the 250–300-nm spectral region, but the 297-nm difference spectral trough suggests a red shift for the denatured azurin Trp absorption band. The Trp ^1L_b transition is thought to be solvent insensitive, while the ^1L_a transition shows significant sensitivity to solvent environment.[28] The disappearance of the sharp 0–0 ^1L_b transition in denatured azurin may result from a red shift of the ^1L_a transition to overlap the ^1L_b transition.

The short-wavelength 232.5-nm maximum in the holo minus apo difference spectrum (Figure 5B) indicates that the apoazurin Trp ^1B_b transition blue shifts. A similar but inverted feature at ca. 230 nm representing a ^1B_b red shift is not completely obvious in the holoazurin minus denatured azurin difference spectrum, but it probably is indicated by the 227-nm shoulder. The Trp spectral changes are masked by the extensive changes in the amide $\pi \rightarrow \pi^*$ transition upon the protein unfolding.

The Trp ^1B_b electronic transition (ca. 220 nm in water and downshifted to 224 nm in organic solvents) is not clearly resolved in the holoazurin, apoazurin, or denatured azurin absorption spectra due to interfering absorbances from tyrosine, phenylalanine, cysteine and histidine, and the amide $\pi \rightarrow \pi^*$ transitions of the protein backbone. The assignment of the 232.5-nm difference spectral feature (Figure 5B) to Trp is consistent with both the modeled difference spectra in Figure 4, A and B, and with the expected ratio[31] of the Trp ^1B_b to ^1L_b absorption spectral changes. We assign this feature to a Trp absorption spectral shift because Trp has a 4-fold greater absorptivity than does Tyr in this spectral region. The red shift of this feature in the protein relative to that for the aqueous difference spectra of Figure 4, A and B, derives from the well-known Trp absorption red shifts in nonpolar solutions. This 232.5-nm feature (Figure 5B) suggests a blue shift of the ^1B_b Trp transition in apoazurin relative to that in holoazurin. In contrast, red shifts are indicated by a trough in Figure 3 (inset) and a shoulder in Figure 5C for the reduced and denatured azurins, respectively. We note that the observed 9.6 ratio for changes in the molar absorptivities of the holoazurin minus apoazurin difference spectrum of the 232.5- and 293.5-nm maxima is within the 6.6–12 range Bailey et al.[31] find for the $\Delta\epsilon_{Bb}/\Delta\epsilon_{L1}$ ratios for Trp methyl ester hydrochloride from difference spectra between organic solvents and water. Similar studies of tyrosine methyl ester hydrochloride give ratios of 3.7 to 5.5.[31] Bailey et al. suggest that any deviations of molar absorptivity change ratios observed in proteins from the ranges observed in the solvent studies indicate additional specific interresidue interactions other than simple dielectric constant and hydrogen bonding differences.[31-33]

If we assume that the entire ca. 233 nm holo minus apo difference spectral feature derived from a Trp blue shift without any bandshape change, we can use the numerically calculated relationship between the magnitude of $\Delta\epsilon_{Bb}/\Delta\epsilon_{Lb}$ and the wavelength shift (Figure 4A) to estimate that the ^1B_b transition of holoazurin is shifted ca. 2 nm to longer wavelength compared to apoazurin.

(31) Bailey, J. E.; Beaven, G. H.; Chignell, D. A.; Gratzer, W. B. *Eur. J. Biochem.* **1968**, *7*, 5–14.
(32) Donovan, J. W. *Biochemistry* **1965**, *4* (5), 823–829.
(33) Benesch, R. E. *J. Am. Chem. Soc.* **1955**, *77*, 5877.

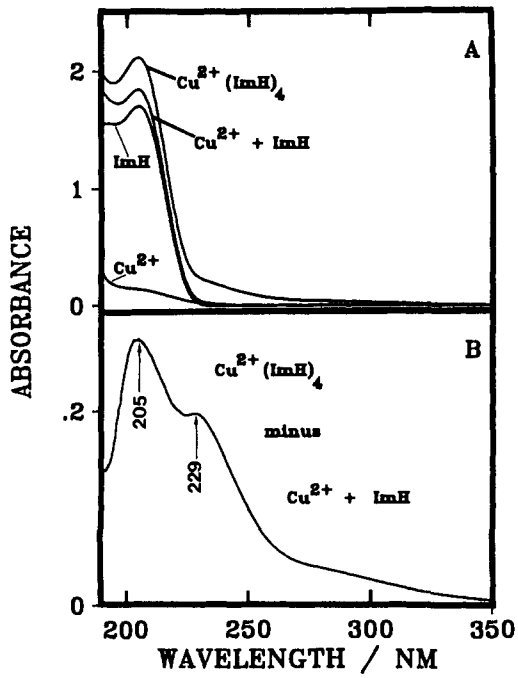

Figure 6. Absorption spectra of aqueous solutions of $Cu^{2+}Cl_2$ (8.75×10^{-4} M), imidazole (ImH, 3.5×10^{-3} M), and Cu^{2+}-$(ImH)_4$ complex (8.75×10^{-4} M). (B) Difference spectrum between the Cu^{2+}-$(ImH)_4$ complex spectrum and the sum of the Cu^{2+} and ImH spectra.

We examined the effect of ligation on the histidine electronic transitions by comparing the absorption spectra of Cu(II)-(imidazole)$_4$ complex to the sum of separate absorption spectra of Cu(II) and imidazole at stoichiometrically identical concentrations (Figure 6A). The difference spectrum in Figure 6B clearly indicates a maximum at 205 nm which derives from a 15% increased absorbance in the complex and a smaller maximum at 229 nm which derives from a 5-fold increased absorbance. Thus, Cu(II) ligation is associated with an increased oscillator strength in the UV region where the Trp ^1B_b transition occurs. We note that the recent Förster energy-transfer calculations of Hansen et al.[6] indicate that a Cu-His transition is a likely candidate for an energy transfer acceptor from the Trp energy donor.

Quantitative Resonance Raman. We report quantitative UVRR cross sections for Trp in holoazurin, apoazurin, and denatured azurin. These values are determined from relative Trp to internal standard Raman intensity ratios extrapolated to zero flux as stated previously. The use of quantitative resonance Raman cross sections enables us to obtain information on the environment of selected chromophores in the azurins with vibrational resolution. Figure 1, which shows the 225-nm Raman spectra of holoazurin, apoazurin, and denatured azurin, indicates that the Raman cross sections of Trp depend upon the azurin conformation and the presence of Cu. The 755-, 1007-, and 1554-cm^{-1} bands derive from the Trp indole ring vibrations.[34] The ca. 1610-cm^{-1} band derives mainly from tyrosine while the 605-cm^{-1} feature derives from the internal standard, cacodylic acid. The Raman cross section values for the 755- and 1007-cm^{-1} bands of Trp in the azurins are displayed in Table I along with cross sections of the Trp monomer.[35] Within the ±4-cm^{-1} spectral resolution, the frequencies of the 755-, 1007-, and 1554-cm^{-1} bands do not change upon protein denaturation or copper removal. The frequencies of these bands are known to be relatively insensitive to environment. Removal of the Cu to form apoazurin increases all of these Trp band resonance Raman cross sections by ca. 30%. Denaturation of holoazurin also removes the copper, but the Raman cross sections are essentially identical with those of holoazurin.

A significant frequency shift occurs for the 1354-cm^{-1} Trp band, the center of which shifts down ca. 20 cm^{-1} to 1335 cm^{-1} in denatured azurin. This band derives from a Fermi resonance between the fundamental N_1–C_8 stretching mode of the indole ring (W7) and combinations of out-of-plane indole ring bending vibrations (W25 + W33 and/or W28 + W29).[36,37] The relative intensity of this doublet strongly depends upon the Trp environment. In the denatured protein the lower frequency component dominates. Very hydrophobic environments show narrow bands with maxima around 1350 cm^{-1} similar to that observed here for holoazurin and apoazurin. This result confirms the absorption spectral result which indicated similar extremely hydrophobic Trp environments for both holoazurin and apoazurin. On the other hand, the denatured azurin Trp environment is significantly altered and has become more hydrophilic as evidenced by the shift of the band center to lower frequency to ca. 1335 cm^{-1}. Due to the overlap with the other broad band centered at ca. 1260 cm^{-1} we cannot directly calculate the ratio of the intensity at 1335 cm^{-1} compared to 1354 cm^{-1}, in order to quantitatively estimate the hydrophobicity of the environment.

The 1150–1300-cm^{-1} spectral region has contributions from the amide III vibration which occurs at ca. 1260, 1280, and 1250 cm^{-1} in the random coil, α-helix, and β-sheet forms. The feature at ca. 1175 cm^{-1} mainly derives from a Tyr vibration. A band at 1277 cm^{-1} derives from cacodylic acid.[21] The 1150–1300-cm^{-1} region is almost identical for the azurin and apoazurin proteins which indicates little change in secondary structure. The increased intensity in the denatured protein in this region may indicate a change in secondary structure.[38,39]

Discussion and Conclusions

The measured azurin Trp UVRR cross sections indicate a decreased Raman cross section in holoazurin compared to apoazurin. Although the absorption data may be subject to error due to uncertain protein concentrations, the Figure 5B absorption difference spectra indicate significant absorbance changes in the region of 225 nm, the Raman excitation wavelength. The Raman excitation wavelength, 225 nm, should be just to the blue side of the Trp excitation profile maximum; the excitation profile maximum for Trp in azurin should be at 228 nm (i.e. 4-nm red shifted[35] from the likely 224-nm Trp ^1B_b absorption maximum of the holoazurin protein). The ca. 2-nm red shift of the ^1B_b transition to the red in the holo relative to the apo could result in as much as a 30% decreased Raman cross section in the holoazurin compared to the apoazurin; the Trp Raman excitation profile is quite narrow.[35]

Our Raman cross section and absorption data suggest electronic coupling between the Trp and the liganded Cu complex:

1. The fluorescence of Trp in holoazurin is quenched compared to apoazurin or denatured azurin. This quenching is shown by the Raman saturation study to derive from fast T_1 nonradiative repopulation of the ground state and presumably derives from a fast energy transfer to the Cu(II) liganded complex. The time scale determined for Trp ground-state recovery is inconsistent with Trp radical cation formation.

2. There appears to be little secondary and tertiary structural difference between holoazurin and apoazurin as evident from the lack of changes in the amide III Raman bands. This result is consistent with previous IR[38] and NMR[40] studies.

3. Reduction of the azurin Cu(II) to Cu(I) results in a ca. 1 nm red shift of the Trp 0–0 ^1L_b transition. A new absorption band probably due to the Cu(I) liganded complex appears at 242 nm. Little change in protein structure is expected from the Cu oxidation state change.

(34) Hirakawa, A. Y.; Nishimura, Y.; Tadashi, M.; Nakanishi, M.; Tsuboi, M. *J. Raman Spectrosc.* **1978**, *7*, 282.
(35) Sweeney, J. A.; Asher, S. A. *J. Phys. Chem.* **1990**, *94* (12), 4748–4791.
(36) Miura, T.; Takeuchi, H.; Harada, I. *J. Raman Spectrosc.* **1989**, *20* (10), 667.
(37) Harada, I.; Takeuchi, H. In *Spectroscopy of Biological Systems*; Clark, R. J. H., Hester, R. E., Eds.; Wiley: New York, 1986; Vol. 13, pp 157–159.
(38) Surewicz, W. K.; Szabo, A. G.; Mantsch, H. H. *Eur. J. Biochem.* **1987**, *167*, 519–523.
(39) Song, S.; Asher, S. A. *J. Am. Chem. Soc.* **1989**, *111*, 4295–4305.
(40) Hill, H. A. O.; Smith, B. E. *J. Inorg. Biochem.* **1979**, *11*, 79–93.

4. The holoazurin Trp ^1L_b absorption band red shifts ca. 1 nm compared to apoazurin, while the ^1B_b transition red shifts ca. 2 nm. The hydrophobicity of the Trp environment appears little changed between Cu(I) azurin, Cu(II) azurin, and apoazurin as evidenced by the narrowness of the Trp ^1L_b 0-0 bands and from the Raman band shape for the Trp 1354-cm^{-1} band. The Trp 0-0 ^1L_b absorption spectral shifts most likely derive from subtle environmental changes, possibly alterations at sites somewhat distant from the Trp ring, such as alterations in electrostatic interaction from the Cu site.

5. The absorption difference spectra (oxidized minus reduced as well as holoazurin minus apoazurin) show large changes in the 200-300-nm spectral region which presumably derive from alterations in sulfur and imidazole → Cu(II) charge-transfer transitions. Numerous charge-transfer transitions can occur since the Cu is ligated to two histidines, one cysteine, and one methionine; simple Cu(II)-(imidazole)$_4$ complexes show increased absorbances throughout the 200-300-nm spectral region (Figure 6).

We thus conclude that facile energy transfer between the Trp and the Cu-ligand complex is responsible for the fluorescence quenching in Trp. Presumably this quenching occurs between the Trp $^1L_{a,b}$ states and a Cu-ligand charge-transfer state. In addition, the Trp absorption spectral shifts between the Cu(I) azurin, Cu(II) azurin, and apoazurin suggest intimate coupling between the electronic transitions of the Cu-ligand complex and those of Trp. It is possible that strong excitonic interactions are present.

Registry No. Trp, 73-22-3; His, 71-00-1; Cu, 7440-50-8.

A Molecular Model for the Major Conformational Substates in Heme Proteins†

Eric Oldfield,*,‡ Kermin Guo,‡ Joseph D. Augspurger,§ and Clifford E. Dykstra§

Contribution from the Department of Chemistry, 505 South Mathews Avenue, University of Illinois at Urbana-Champaign, Urbana, Illinois 61801, and Department of Chemistry, 1125 East 38th Street, Indiana University-Purdue University at Indianapolis, Indianapolis, Indiana 46205.
Received October 22, 1990

Abstract: We present a molecular model of the major "conformational substates" observed by infrared spectroscopy in carbonmonoxyhemoglobins, myoglobins, and peroxidases, in terms of an electrical perturbation of the CO fundamental vibrational frequencies due to the possibility of $H^{\epsilon 2} \leftrightarrow H^{\delta 1}$ tautomerism, and 180° C^{β}-C^{γ} ring flips, of distal histidine residues. The model supports a previous interpretation of vibrational frequencies and nuclear magnetic resonance chemical shifts of CO ligands in heme proteins as originating in a weak electric field (dipole and quadrupole interactions with permanent dipole moments, dipole polarizabilities, and shielding polarizabilities), and opens up the possibility of future detailed molecular interpretations of both NMR chemical shifts (of ^1H, ^{13}C, and ^{15}N), as well as IR data, on proteins and other macromolecules.

Conformational substates (CS) in heme proteins, as evidenced by both infrared (IR) spectroscopy[1,2] and X-ray crystallography,[3] have been a topic of considerable interest for many years, and great emphasis has been placed on investigating the heme proteins carbonmonoxyhemoglobin and carbonmonoxymyoglobin. Much valuable information has been obtained from such studies, but no entirely satisfactory molecular model for the individual CSs has been forthcoming. We propose in this paper a molecular model that appears to rationalize the observation of numerous substates in a wide variety of heme proteins, including the hemoglobins, myoglobins, and several peroxidases. Our model is extremely simple, and involves electric field induced frequency shifts due to 180° ring flips of the $H^{\delta 1}$ and $H^{\epsilon 2}$ tautomers of distal histidine residues.

Recently, we have been investigating the ^{13}C and ^{17}O nuclear magnetic resonance (NMR) spectra of ^{13}CO and $C^{17}O$ ligands in a series of carbonmonoxyheme proteins, as a prelude to an investigation of the long-standing general problem of the nature of the chemical shift nonequivalences seen in proteins, and we have found an excellent correlation between the isotropic chemical shieldings, $\delta_i(^{13}C)$ and $\delta_i(^{17}O)$, and the mean fundamental vibration frequency, ν_{CO},[4] of the heme's CO ligand. Our observations, and additional correlations with ν_{FeC}, and with the $C^{17}O$ nuclear quadrupole coupling constant, e^2qQ/h, were explained in terms of a "back-bonding" model.[4] However, there seems to be a more fundamental and quantitative basis for the correlations between the chemical shifts, CO vibrational frequencies, and the nuclear quadrupole coupling constants.

Calculations we have carried out suggest that the perturbation of heme-CO by other ligands is largely electrical in nature.[5] This is consistent with the idea that the primary electronic structure change in a molecule from perturbation of a nearby, but not chemically bonded, molecule is charge polarization.[6] This idea has provided a basis for a general, weak interaction model,[7] and it was employed in our recent study[5] of carbonmonoxyheme proteins. We calculated the effect on the vibrational potential and the chemical shielding tensors due to a range of electrical potentials that arise from a nearby point dipole and point quadrupole. The result was that we were able to suggest an explanation for the general trends seen in the heme proteins: a $\delta_i(^{13}C)$ increase, $\delta_i(^{17}O)$ decrease, $e^2qQ/h(^{17}O)$ decrease, and ν_{CO} decrease, in terms of the interaction of CO with an electric field. Although the

† This work was supported by the United States Public Health Service (Grants NIH HL-19481 and GM 40426-03).
‡ University of Illinois at Urbana-Champaign.
§ Indiana University-Purdue University at Indianapolis.

(1) Ansari, A.; Berendzen, J.; Braunstein, D.; Cowen, B. R.; Frauenfelder, H.; Hong, M. K.; Iben, I. E. T.; Johnson, J. B.; Ormos, P.; Sauke, T. B.; Scholl, R.; Schulte, A.; Steinbach, P. J.; Vittitow, J.; Young, R. D. *Biophys. Chem.* **1987**, *26*, 337-355.
(2) Potter, W. T.; Hazzard, J. H.; Choc, M. G.; Tucker, M. P.; Caughey, W. S. *Biochemistry* **1990**, *29*, 6283-6295.
(3) Kuriyan, J.; Wilz, S.; Karplus, M.; Petsko, G. A. *J. Mol. Biol.* **1986**, *192*, 133-154.
(4) Park, K. D.; Guo, K.; Adebodun, F.; Chiu, M. L.; Sligar, S. G.; Oldfield, E. *Biochemistry* **1991**, *30*, 2333-2347.
(5) Augspurger, J. D.; Dykstra, C. E.; Oldfield, E. *J. Am. Chem. Soc.* **1991**, *113*, 2447-2451.
(6) Dykstra, C. E. *Acc. Chem. Res.* **1988**, *21*, 355-361.
(7) Dykstra, C. E. *J. Am. Chem. Soc.* **1989**, *111*, 6168-6174; *J. Phys. Chem.* **1990**, *94*, 6948-6956.

0002-7863/91/1513-7537$02.50/0